doi:10.1016/j.jmb.2008.12.036 J. Mol. Biol. (2009) 387, 407–415

JMB

Available online at www.sciencedirect.com

ScienceDirect

ELSEVIER

Amyloid Aggregation on Lipid Bilayers and Its Impact on Membrane Permeability

Ran Friedman, Riccardo Pellarin* and Amedeo Caflisch*

Department of Biochemistry, University of Zürich, Winterthurerstrasse 190, CH-8057 Zürich, Switzerland

Received 29 October 2008; received in revised form 15 December 2008; accepted 16 December 2008
Available online 24 December 2008

Fibrillar protein aggregates (amyloids) are involved in several common pathologies, e.g., Alzheimer's disease and type II diabetes. Accumulating evidence suggests that toxicity in amyloid-related diseases originates from the deposition of protein aggregates on the cell membrane, which results in bilayer disruption and cell leakage. The molecular mechanism of damage to the membrane, however, is still obscure. To shed light on it we have performed coarse-grained molecular dynamics simulations of fibril-forming amphipathic peptides in the presence of lipid vesicles. The simulation results show that highly amyloidogenic peptides fibrillate on the surface of the vesicle, damaging the bilayer and promoting leakage. In contrast, the ordered aggregation of peptides with low amyloidogenicity is hindered by the vesicles. Remarkably, leakage from the vesicle is caused by growing aggregates, but not mature fibrils. The simulation results provide a basis for understanding the range of aggregation behavior that is observed in experiments with fibril-forming (poly)peptides.

Keywords: protein aggregation; Alzheimer's disease; diabetes type II; membrane leakage; coarse-grained; molecular dynamics

Edited by D. Case

Introduction

Amyloid-related diseases such as Alzheimer's, Parkinson's and type II diabetes are characterized by the presence of protein aggregates in one or more tissues. These protein aggregates are assembled into well-ordered filamentous, β-sheet-rich structures[1–6] termed amyloid fibrils. Compelling evidence suggests that oligomeric or other prefibrillar precursors of amyloid fibrils are the main toxic species,[7–9] but the mechanism of cell and tissue damage in amyloid-related diseases is poorly understood. The interactions of amyloidogenic polypeptides with the cell membrane can accelerate fibril formation and are reported to be involved in the toxicity of oligomers or protofibrils.[10,11] Furthermore, amyloid peptides not only aggregate on the lipid surface, but also penetrate into membranes.[12,13] The accumulation of amyloid peptides destabilizes lipid bilayers and alters their permeability,[14,15] which may contribute to cell damage and toxicity. Accordingly, recent biophysical studies have targeted the interactions of amyloid aggregates with lipid vesicles.[16–18] These studies have provided evidence that the formation of fibrils on a membrane damages the bilayer's integrity.

The fibrillation process is dynamic and transient, making it difficult to explain the mechanism of aggregation based on experimental evidence alone. Many efforts have therefore been made to study protein and peptide aggregation by computational methods and in particular molecular dynamics simulations, as reviewed in Refs. 19 and 20. Atomistic simulations of proteins are limited to the time scale of 10–100 ns, which is not enough to simulate aggregation or even oligomerization. Accordingly, there is a need to reduce the complexity, e.g., by investigation of oligopeptide systems[21–27] or by use of simplified models. Recently, a coarse-grained model of amphipathic peptides has enabled the simulation of amyloid fibril formation and the analysis of aggregation pathways and kinetics, which were observed to depend on the intrinsic amyloidogenic tendency of the peptide.[28,29] The peptide monomer has a single degree of freedom. Its free-energy profile has two minima corresponding to the amyloid-competent and amyloid-protected states. The peptides can fibrillate only in the former

*Corresponding authors. E-mail addresses: pellarin@bioc.uzh.ch; caflisch@bioc.uzh.ch.

Abbreviations used: LJ, Lennard-Jones.

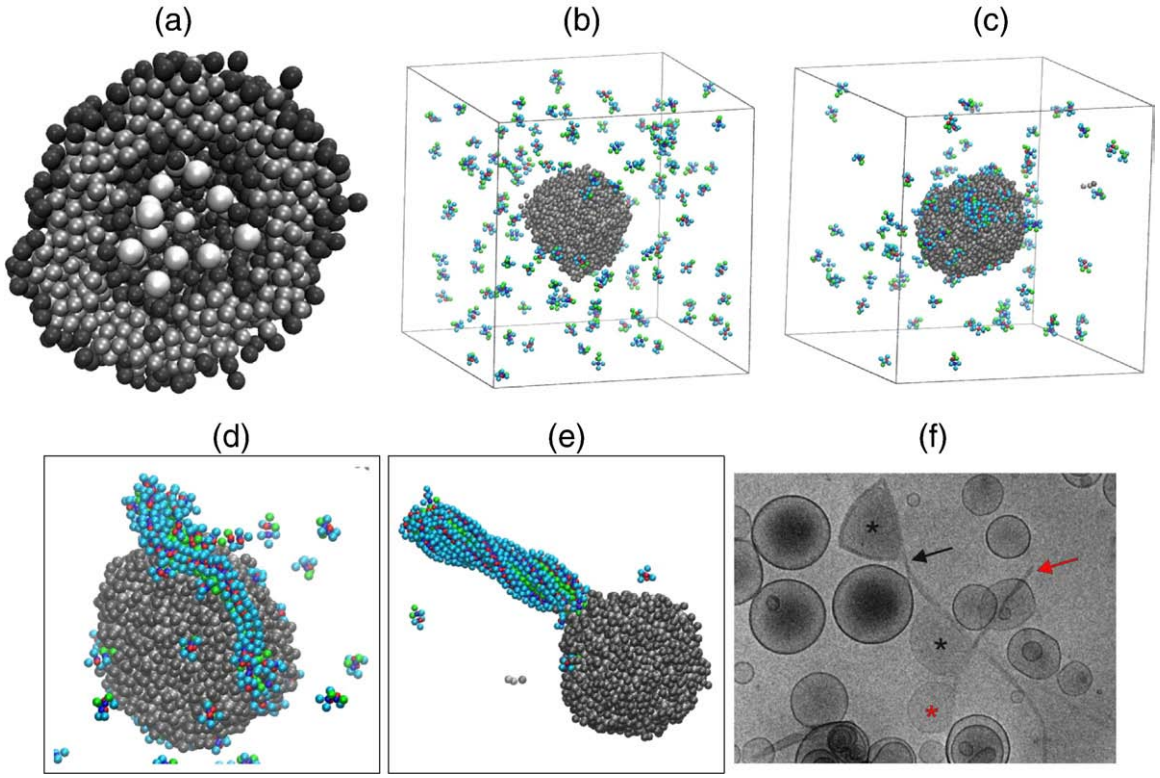

Fig. 1. Aggregation on the surface of a vesicle. (a) A cut through a lipid vesicle showing probe spheres in the inner space. The two-bead hydrophobic tail and one-bead hydrophilic head of the lipids are colored gray and black, respectively; probe spheres are shown in white. (b–e) Snapshots from a simulation of peptides with intermediate amyloidogenicity (see subsection "Coarse-grained model of amphipathic peptide") at times 0 (b), 10 (c), 125 (d), and 700 ns (e). Peptide beads are color coded according to their type: hydrophobic in green, hydrophilic in cyan and dipoles in red and blue. Details about the peptide model are given in Refs. 28 and 29. (f) Cryotransmission electron microscopy of the interaction between human islet amyloid polypeptide and unilamellar phospholipid vesicles (reproduced with permission from Ref. 18). Few vesicles (asterisks) are in contact with fibrils (arrows). Note the similar relative orientation of the fibril and the vesicle in the simulations (e) and electron microscopy image (f), in particular the vesicle and fibril marked in red.

conformation. Hence, the amyloidogenic potential corresponds to the free-energy difference between the two states. Here, we use a novel coarse-grained model of a bilayer-forming lipid (the lipid molecules spontaneously assemble into spherical, unilamellar bilayer vesicles; see Fig. 1a), together with the previously developed amphipathic peptide model, to study the amyloid aggregation on lipid vesicles. The goal of the simulation study is twofold: to analyze the influence of the vesicles on the aggregation mechanism and to analyze the effect of aggregation on the structure and permeability of the lipid bilayer.

Results and Discussion

Multiple independent simulations were performed for each of four types of amphipathic peptides having high, intermediate, low or very low amyloidogenic potential (see Table 1). Note that the interaction energy between the monomeric peptide and the lipids is similar for the amyloid-prone and amyloid-protected conformations.

Fibrillation on the vesicles

Four snapshots from a simulation of peptides with intermediate amyloidogenic potential are depicted in Fig. 1b–e. Upon starting the simulation, about half of the peptides quickly adsorb to the vesicle surface. The initial adsorption does not depend on the amyloidogenicity because of the aforementioned similar hydrophobic interactions between the lipids and amyloid-prone or amyloid-protected peptide conformations. Peptide adsorption is followed by transient formation of small oligomeric species (2–10 peptides) within tens of nanoseconds (Figs. 1c and 2). Peptide monomers and oligomers subsequently form larger aggregates with filament characteristics, i.e., a file of ordered peptides (Fig. 1d), before their maturation into a fibrillar structure (Fig. 1e, note the similarity to electron microscopy of amyloid fibrils attached to the surface of vesicles; Fig. 1f; Ref. 18).

Highly amyloidogenic peptides fibrillate more rapidly in the presence of lipid vesicles than in their absence, while the opposite is observed for peptides of low amyloidogenicity (half-times of fibril formation are given in Table 1). The faster

Table 1. Simulation details, including characteristic half-times for fibrillation and leakage

Amyloidogenicity[a]	No. of simulations	Fibrillation, $t_{50} \pm$ SD (ns)[b]	Leakage, $t_{50} \pm$ SD (ns)[c]
No vesicles			
High	97	19 ± 3	
Intermediate	99	56 ± 15	
Low	100	124 ± 28	
Very low	90	304 ± 110	
With vesicles			
High	10	11 ± 1	123 ± 89
Intermediate	29	89 ± 29	175 ± 124
Low[d]	20	958 ± 503	444 ± 178
Very low	30	>1000	503 ± 171
Only vesicles	10		2875 ± 2064[e]
Vesicles and preformed fibrils			
Intermediate	10		2123 ± 960[e]

The simulations were run for 1 μs unless otherwise stated.
[a] Amyloidogenicity is determined by dE. A value of dE=0 kcal/mol corresponds to high, −1.5 to intermediate, −2.0 to low and −2.25 to very low amyloidogenicity.
[b] The rate of fibrillation is quantified by the half time of fibril formation, t_{50}. The value of t_{50} is defined as the simulation time required for the formation of a fibril with 100 polar contacts, since there are 200–250 polar contacts between the peptides (each peptide can make two polar contacts with adjacent peptides and the total number of peptides in the simulations is 125).
[c] The average time needed for 50% of the probes to escape from the vesicle.
[d] Of 20 runs, 17 were elongated to 2 μs. In 3 runs, no nucleation event occurred even after 2 μs.
[e] These values are extrapolated from an exponential best fit of individual kinetic traces.

aggregation kinetics of highly amyloidogenic peptides is a consequence of their higher effective concentration on the lipid bilayer relative to the bulk.[10,30] In contrast, despite the same increase of peptide concentration on the vesicle surface, fibrillation of peptides with low amyloidogenic potential is slower in the presence of lipid vesicles. It has previously been shown that peptides with low amyloidogenic potential can fibrillate only after aggregating into spherical oligomeric intermediates with hydrophobic interior and hydrophilic surface.[28] In the simulations with lipids, such oligomeric intermediates form in the bulk but not on the vesicle (Fig. 2, green histogram). Fibrillation of low-amyloidogenicity peptides therefore takes place in the bulk and is slower than in the absence of a vesicle due to the lower effective concentration of peptides in the solvent. These simulation results are consistent with and explain the apparently contradictory experimental observations on faster aggregation of the Aβ[17] or α-synuclein[13] peptides in the presence of lipid surfaces and slower aggregation of insulin (which has lower amyloidogenicity).[31]

Growing aggregates promote leakage from vesicles

Several experimental works indicate that the process of fibrillation on the bilayer surface is responsible for membrane perturbation.[32,33] Recently, membrane damage was assessed by monitoring the kinetics of fluorescent probe release from vesicles.[18] Inspired by this experimental technique, we have simulated vesicles that initially encapsulate 20 inert probe spheres (Fig. 1a) for monitoring the release of the probes to the bulk in the presence or absence of peptides. Strikingly, leakage from vesicles is enhanced by the aggregation of the peptides in all simulations. A comparison between the fibrillation and probe release rates (Fig. 3a and b) reveals that probe release is fastest during fibril growth. Moreover, the higher the tendency of the peptide to form fibrils, the faster the leakage (Fig. 3b and Table 1). The probes are released by sporadic events (Figs. 4 and 5), which indicates that the damage to the lipid bilayer is due to transient formation of surface defects (ruptures), as previously suggested on the basis of atomic force microscopy experiments.[34] The formation of defects on the vesicle's surface is exemplified in Fig. 3c and d by a snapshot from a simulation showing a transient bilayer rupture. Examination of the simulations reveals that the membrane surface defects are formed during the growth, on the bilayer, of multiple filaments or a

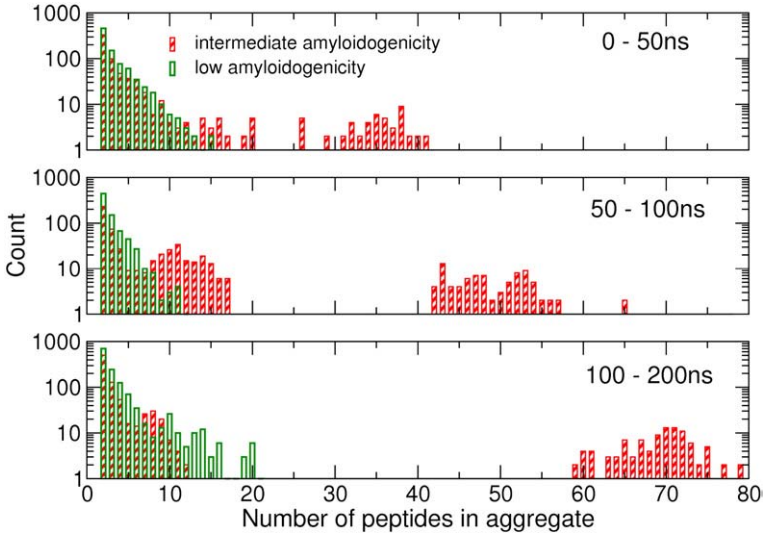

Fig. 2. Histograms of the sizes of the peptide aggregates on the vesicle. Peptides with intermediate amyloidogenicity (red) form aggregates of increasing size on the membrane, whereas low-amyloidogenicity peptides (green) form only very few aggregates with more than 10 monomers (note the logarithmic scale on the y-axis). The probability that aggregates will form (for peptides with low amyloidogenicity) decreases with the size of the oligomer, which indicates that the aggregates are formed only by collision of monomers and that no metastable oligomers are observed.[28]

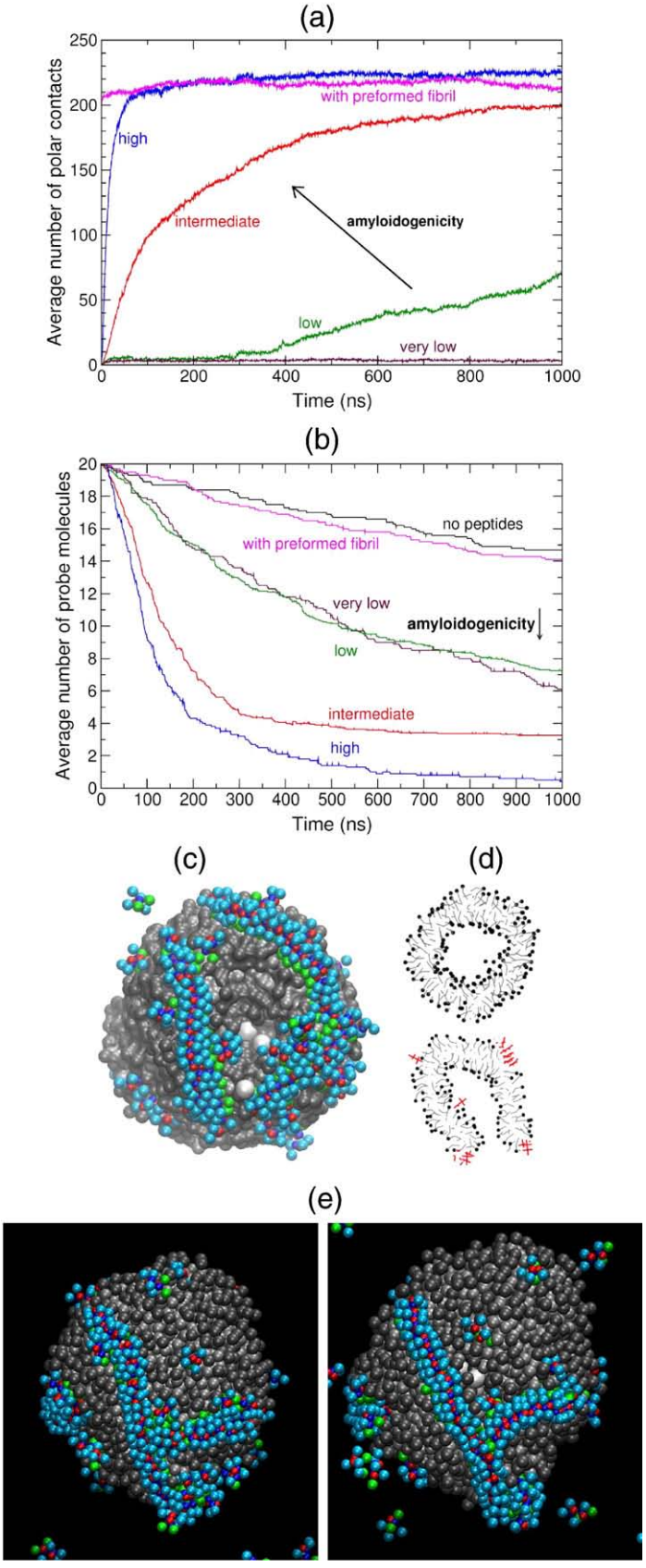

Fig. 3. The impact of peptide amyloidogenicity on fibril growth kinetics and vesicle leakage. A single parameter, the energy difference between amyloid-competent and amyloid-protected conformations of the peptides, is varied in different simulations to tune amyloidogenicity (see Materials and Methods). (a) Time series of the average number of ordered polar contacts between monomers (corresponding to the degree of fibrillation[28]). (b) Average number of probes inside the vesicle, in the absence (black) or presence of peptides (colors) and for simulations where a preformed fibril was used instead of dispersed peptides. (c) A snapshot from a simulation, showing the escape of probes from inside the vesicle. Peptides and lipids are colored as in Fig. 1. Three probe molecules (white spheres) are visible; one has just escaped from the vesicle, two others are located in the vesicle but are visible because of a defect in the bilayer. (d) A two-dimensional section through a vesicle, in the absence (top) or presence of adsorbed peptides (bottom). The section in the bottom of (d) corresponds to a vertical plane cut through the vesicle shown in (c). Lipid tails and head groups are presented as gray sticks and black spheres, respectively, and peptides as red sticks. (e) An example of vesicle rupture. Snapshots just before (left) and during (right) rupture of the vesicle, showing a branched Y-shaped filament (formed by peptides of intermediate amyloidogenicity) that grows on the membrane. Note that a branched filament is an unstable structure formed by the transient Y-shaped association of two filaments on the vesicle surface during the fibrillation process.

transiently branched filament (Fig. 3c–e). It should be noted that the release of probe spheres due to isolated peptides and small oligomeric species on the vesicle surface is still faster than in the absence of peptides (Fig. 3b), revealing that the amphipathic monomers and nonfibrillar oligomers can also

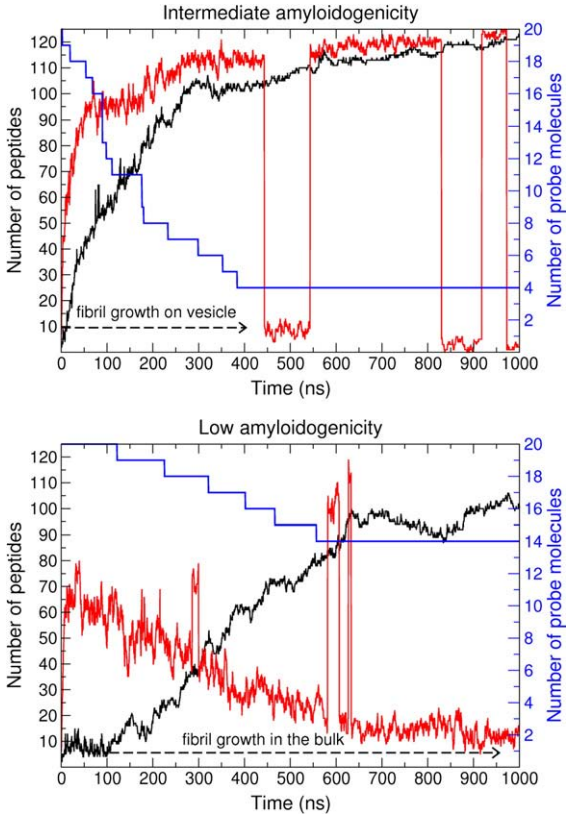

Fig. 4. Fibril growth on the vesicle surface promotes membrane leakage. Time series of the size of the largest peptide aggregate (black), the number of peptides attached to the vesicle as monomers or aggregates (red), and the number of probes inside the vesicle (blue, corresponding to the axis on the right). (Top) For peptides with intermediate (shown) or high (not shown) amyloidogenicity, the size of the largest aggregate and the number of peptides on the bilayer surface increase concomitantly, indicating that the fibril is formed on the surface of the vesicle. During fibril growth, there is fast leakage of the probes from the vesicle. The binding of the fibril is reversible: after about 400 ns, the largest aggregate has >110 peptides, and it can detach from the vesicle (shown as jumps in the red trace). (Bottom) In contrast, when amyloidogenicity is low, the number of peptides on the vesicle decreases, while the size of the largest aggregate grows, indicating that the fibril is formed in the bulk (although it occasionally binds to the vesicle surface). The release of probes from the vesicle is slower when amyloidogenicity is low. In both cases, other simulations with different initial distribution of velocities show similar behavior, although the details (e.g., length of the lag phase and number of probes in the vesicle at the end of the run) can differ.

damage the membrane, as implied by atomic force microscopy and membrane-conductance experiments.[34,35] In striking contrast to the faster leakage due to fibril growth, the kinetics of probe release in the presence of mature fibrils are as slow as in the absence of peptides (Fig. 3b), indicating that mature fibrils do not damage the integrity of the vesicle. Rather, the ongoing process of aggregation on the vesicle results in bilayer surface defects (see Fig. 6 for a schematic presentation). This observation explains why for some amyloidogenic peptides there exist mutants that form fibrils more rapidly and are more toxic than the wild-type peptides, even though their fibrils are not toxic.[8]

Conclusions

The mechanism of membrane damage due to fibril growth during amyloid aggregation has been studied here using coarse-grained molecular dynamics simulations. The results shed light on the molecular mechanism of membrane-associated amyloid aggregation (Fig. 7). At the beginning of the simulations, peptides adsorb to the vesicle and peptide oligomers are quickly formed. Peptides with *low* amyloidogenicity (Fig. 7, left) are characterized by a higher stability of the monomeric state and therefore form only small aggregates on the membrane. Fibril formation takes place in the bulk, where the diffusion of the peptides is faster. When amyloidogenicity is *high* (Fig. 7, right), the initial adsorption to the vesicle is followed by ordered templating due to the high concentration of aggregation-prone peptides on the bilayer surface. The resulting filaments assemble and eventually fibrillate on the vesicle surface. Remarkably, leakage from lipid vesicles is caused primarily by the growth of filaments, which results in transient defects of the membrane. In striking contrast, mature fibrils do not damage the vesicle. The simulation results provide strong evidence that the influence of lipid membranes should be taken into account for the

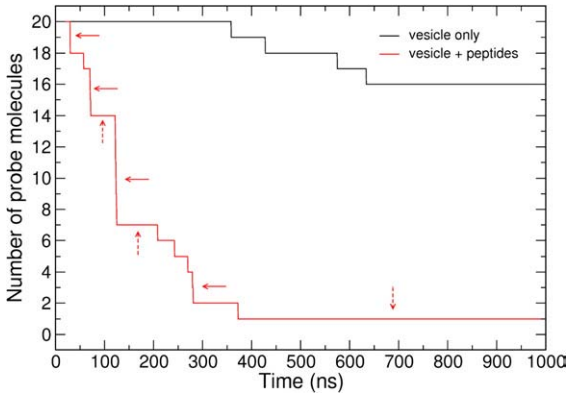

Fig. 5. Transient rupture of the vesicle promotes leakage. The release of probes from vesicles: examples from individual trajectories. The number of probes inside the vesicle is shown as a function of simulation time for two trajectories: in the absence of peptides (black) and in the presence of 125 peptides of intermediate amyloidogenicity in the simulation box (red). Note that in the absence of peptides, probe molecules are released one by one (visible as small steps along the black trace). With peptides, the rate of release is faster but not constant. Several probes are released within a few nanoseconds (shown by horizontal arrows) and then none are released for 50 ns or more (vertical dashed arrows). This behavior indicates that transient vesicle ruptures facilitate leakage.

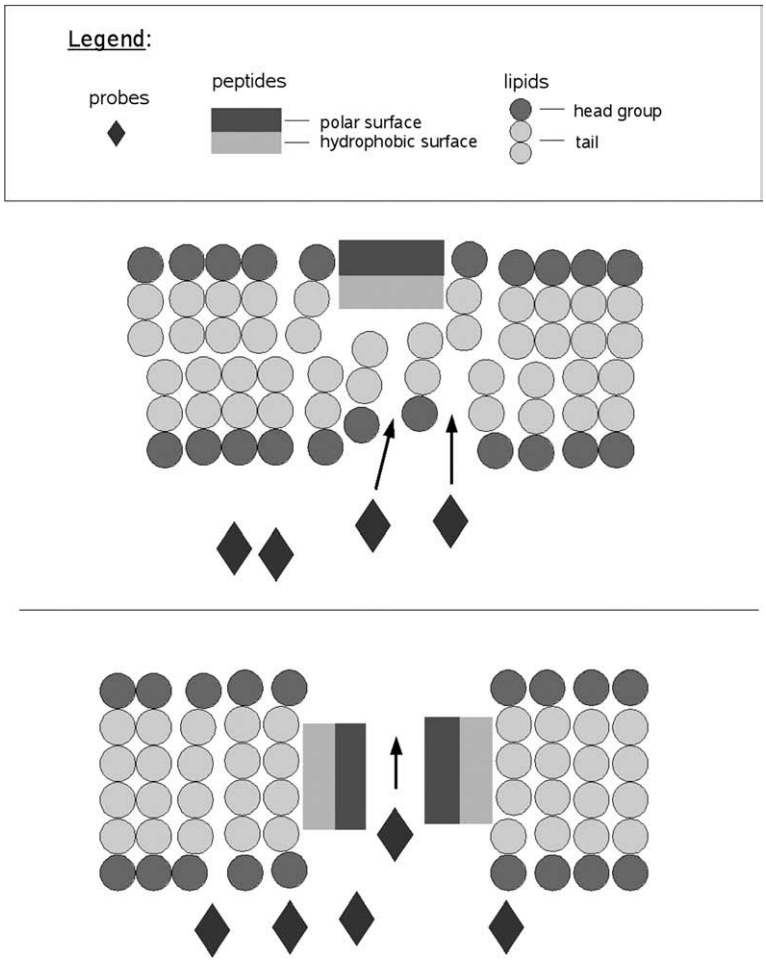

Fig. 6. A schematic presentation of cell leakage due to peptide monomers (top) or growing aggregates (bottom). The hydrophilic and hydrophobic parts of the molecules are shown by dark and light areas, respectively. The upper frame presents a peptide monomer (rectangle) partially inserted into the lipid bilayer. The packing of the lipids around the peptide is not optimal, which results in small gaps through which probes (diamonds) can escape. The lower frame shows peptide monomers (for clarity, only two monomers are shown) that insert into the membrane during aggregation (see, e.g., Fig. 3c–e), oriented with their hydrophobic part towards the lipids. Peptide insertion creates vesicles defects through which probes can rapidly escape.

development of aggregation inhibitors as potential drugs to cure amyloid-related diseases.[36,37]

Materials and Methods

Coarse-grained model of amphipathic peptide

The amphipathic peptide model, as used here, has been described in detail elsewhere.[28,29] Briefly, each peptide monomer consists of 10 beads. Four of the beads carry partial charges of $\pm 0.4e$, thereby generating two dipoles. Four of the uncharged spheres are hydrophilic, and the other two are hydrophobic (Fig. S1). The coarse-grained model of the aggregating peptide does not represent any particular amino acid sequence. Yet, changes in the amyloidogenic tendency of the aggregating monomer yield different polymerization processes and kinetics.[28,29] The conformational landscape of isolated monomers is simplified such that only two states are considered: amyloid competent (β) and amyloid protected (π). In the β state, the parallel orientation of the two intramolecular dipoles favors ordered aggregates with intermolecular dipolar interactions parallel to the fibril axis. Conversely, the π state represents the ensemble of all polypeptide conformations that are not compatible with self-assembly into a fibril (e.g., random coil, partially unfolded or helical). At physiological temperature, the isolated monomer undergoes a reversible isomerization from the π to the β state. The energy difference between these two states, $dE = E_\pi - E_\beta$, can be interpreted as the β-aggregation propensity of a polypeptide. dE is close to the free-energy difference because the peptide has one degree of freedom.[28] For instance, when $dE = 0$ kcal/mol, the π and β states are equally populated, whereas for $dE = -1.5$ and -2.5 kcal/mol, the π state is about 15 and 100 times more populated than the β state, respectively. Here, simulations were performed with the following four values of dE: 0 kcal/mol (high amyloidogenic potential), -1.5 kcal/mol (intermediate), -2.0 kcal/mol (low) and -2.25 kcal/mol (very low). Earlier simulation studies have shown that the aggregation process proceeds directly (without the formation of soluble intermediates) when $dE > -2.0$, whereas with $-2.0 \le dE \le -2.5$, oligomeric intermediates were observed[28] and the energy landscape was far more complex.[29] Note that the β-aggregation propensity dE cannot be directly related to experimental measurements. Yet, it can be derived from relative changes, e.g., upon mutation. For instance, the length of the lag phase in thioflavin T fluorescence kinetic measurements of different mutants might give the relative tendency of sequence variants to fibrillate. Alternatively, folding and aggregation kinetics experiments can be combined to estimate the relative stability of aggregation-competent intermediates and folded conformations.[38]

Coarse-grained model of lipids

The basic lipid model is composed of three beads: a hydrophilic bead, which represents the head group, and two hydrophobic beads, which represent the lipid tail. The connectivity of the beads is shown in Fig. S2. The length of the bonds is 7 Å and the angle between the beads is 134°. The beads do not bear any partial charges. The model is

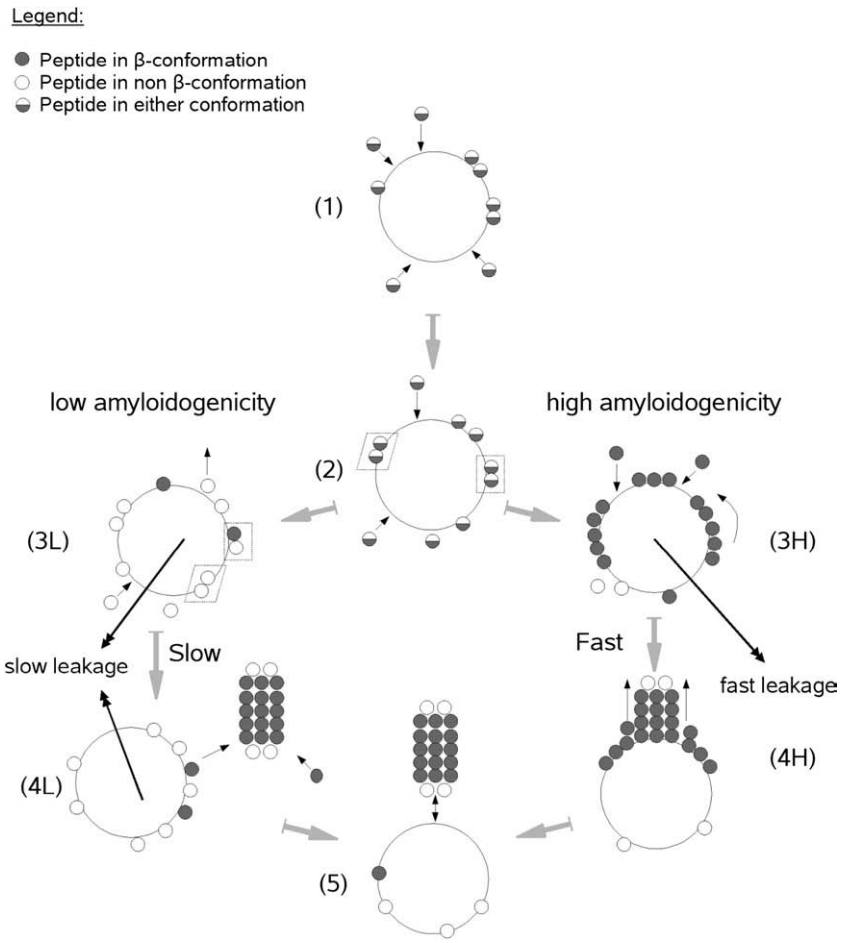

Fig. 7. Schematic representation of peptide aggregation on a vesicle. At the beginning of the simulations (step 1), peptides (small circles) adsorb to the vesicle (large circle). The adsorption of the peptides does not depend on their amyloidogenicity because of similar hydrophobic interactions between the lipids and amyloid-prone or amyloid-protected peptide conformations. Peptide oligomers (enclosed in lines) are quickly formed (step 2, Fig. 1c). When amyloidogenicity is high, aggregation continues by ordered templating due to the high concentration of aggregation-prone peptides (gray) on the bilayer surface. The resulting filaments assemble (step 3H) and eventually fibrillate on the vesicle surface (4H, Fig. 1e). Peptides with low amyloidogenicity are characterized by a higher stability of the amyloid-protected monomeric state (white). Thus, they form only small aggregates on the membrane (3L, see also Fig. 2), while fibril formation takes place in the bulk where the diffusion of the peptides is faster (4L). At the final equilibrium, the mature fibrils can bind and unbind the vesicle surface (step 5).

reminiscent of the lipid unit in a membrane model developed by Cooke and Deserno,[39] but was developed independently and differs in many aspects, e.g., bonded and nonbonded interactions, *vide infra*. In our model, the bonds are constrained by the SHAKE algorithm,[40] the angles are held by a force constant of 100 kcal mol^{-1} deg^{-1}, and nonbonded attraction and repulsion are modeled by the Lennard-Jones (LJ) equation. By tuning the sizes of the beads and the depth of the LJ potential for each bead, one can obtain various lipid arrangements. We set $R_{\text{hydrophilic}}=3.1$ Å, $R_{\text{hydrophobic}}=3.0$ Å, $\varepsilon_{\text{hydrophilic}}=-0.1$ kcal/mol and $\varepsilon_{\text{hydrophobic}}=-1.265$ kcal/mol. Under these conditions, 1000 lipids simulated in a cubic box of 290 Å dimension spontaneously form, within 50 ns, unilamellar vesicles with average bilayer thickness (distance between the head groups) of 28.0 ± 1.2 Å. The vesicles are roughly spherical in shape, as shown in Fig. 1. They have a gyration radius of 43.22 ± 0.19 Å, so that the area per lipid is 64.61 ± 0.47 Å^2 and the volume of the simulation box is roughly 30 times that of the vesicle.

Interactions between lipids and peptides

Interactions between the lipids and the peptides are defined by the LJ potential:

$$V_{ij}(r_{ij}) = \varepsilon_{ij}\left[\left(\frac{r_{ij,\min}}{r_{ij}}\right)^{12} - 2\left(\frac{r_{ij,\min}}{r_{ij}}\right)^{6}\right]$$

where i and j are two atoms belonging to different molecules, r_{ij} is the distance between them, $r_{ij,\min}$ is the distance at which the energy is minimal, and $-\varepsilon_{ij}$ is the energy at that minimum. The equilibrium parameters are given per bead type, i.e., $r_{i,\min}$ and ε_i, and the binary parameters for heteroatoms are calculated as $\varepsilon_{ij}=\sqrt{\varepsilon_i\varepsilon_j}$ and $r_{ij,\min}=(r_{i,\min}+r_{j,\min})/2$. In the present study, electrostatic interactions between lipids and peptides are not taken into account for simplicity. It is likely that the strength of these interactions depends on the composition of the bilayer and that they might be negligible in certain cases, e.g., for zwitterionic (phospho)lipids. It has been shown that some compositions of lipids accelerate fibril formation better than others, which can be attributed to the strength of the interactions between the lipids and the peptide monomers.[16,15] Here, the affinity of the membrane for the peptides is tuned by a coupling parameter, λ, to enable the simulation of membranes with different affinities towards the peptides and lipids. The LJ parameter ε_{ij} is multiplied by λ when i$\in$peptides and j$\in$lipids. Thus, a higher value of λ represents lipid compositions with a higher affinity for the peptides. Different values of λ were tested, and it was observed that values of $0.85<\lambda\leq0.9$ resulted in the initial binding of approximately 50% of the peptides to the lipid vesicle, allowing interactions between peptides both in the bulk and at the surface, as well as partial or (rarely) complete penetration of the peptides into the vesicle. We therefore set $\lambda=0.87$ unless otherwise stated (but see also Table S1).

Assuming that the interactions between amphipathic peptides and lipids are hydrophobic in nature, other atomistic or coarse-grained models that take into account van der Waals interactions could in principle be used for simulations of peptide aggregation on the vesicle surface.

Note that our peptide model shows rather robust aggregation properties (and presence of oligomeric intermediates at $dE = -2.5$ kcal/mol) upon small changes of the parameters, e.g., the van der Waals energy minimum (see the supporting information of Ref. 28).

Simulation protocols

The amyloid aggregation simulations are started by placing a preequilibrated unilamellar bilayer vesicle in a cubic box of 29-nm dimension. The total number of lipids in the box is 1000 (corresponding to a concentration of 68 mM, which is 40 times higher than the critical concentration for vesicle formation of the model). Then, 125 peptide monomers (8.5 mM) are randomly placed in the bulk so that the distance between each peptide and any other molecule is greater than 1.5 nm (Fig. 1b). The system is thereafter minimized, equilibrated and simulated by Langevin dynamics using CHARMM.[41]. The only parameter that differs in different simulations is dE, the energy difference between the amyloid-protected and amyloid-prone conformations of the peptide in its monomeric state. Thus, the more negative the value of dE, the lower the amyloidogenicity, i.e., the lower the tendency of the peptides to aggregate into fibrils (Fig. 3a and Table 1).

Simulations with probe molecules

Probe-release experiments, in which the rate of release of fluorescent molecules is studied in the presence or absence of aggregating peptides, were carried out to evaluate the effect of amyloid peptides on the integrity of lipid bilayers (see, e.g., Ref. 18). Here, the escape of probe molecules is simulated by starting from 20 spherical probes (with a radius of 4.5 Å and mass of 625 Da, which is similar to the mass of calcein, the molecule used in the probe-release experiments[18]) inside a preequilibrated vesicle. The rate of probe release can then be measured in the presence or absence of peptides. The interactions between probe molecules and all other particles (lipids, peptides and probes) are governed solely by the LJ equation. The probe molecules are hydrophilic due to their small (in absolute value) LJ-energy parameter at optimal distance ($\varepsilon = -0.2$ kcal/mol).

Simulations of vesicles with an equilibrated fibril

To evaluate the effect of fibrils on the integrity of vesicles, we ran 10 simulations of vesicles after addition of a preequilibrated fibril. The simulation system consisted of a 1000-lipid vesicle with 20 spherical probes in its interior and 125 peptides (of which 112 were assembled into a fibril and the remaining 13 were dispersed in the bulk). The simulations were carried out as described above for a duration of 1 μs. The fibrils were stable under these conditions, as indicated by a constant number of polar contacts, and no lipid depletion from vesicles was observed in the simulations.

Acknowledgements

The authors thank Dr. M. F. M. Engel, F. Marchand, Dr. S. Muff and Prof. B. Schuler for critically reading the manuscript. The simulations were performed on the Etna and Matterhorn computer clusters at the University of Zürich we are grateful to P. Schütz and C. Bolliger for computer support. This work was supported by the Swiss National Competence Center for Research (NCCR) in Neural Plasticity and Repair, the Swiss National Science Foundation, the Novartis Foundation, and the Research Program for young scientists of the University of Zürich.

Supplementary Data

Supplementary data associated with this article can be found, in the online version, at doi:10.1016/j.jmb.2008.12.036

References

1. Sunde, M. & Blake, C. (1997). The structure of amyloid fibrils by electron microscopy and X-ray diffraction. *Adv. Protein Chem.* **50**, 123–159.
2. Petkova, A., Ishii, Y., Balbach, J., Antzutkin, O., Leapman, R., Delaglio, F. & Tycko, R. (2002). A structural model for Alzheimer's beta -amyloid fibrils based on experimental constraints from solid state NMR. *Proc. Natl Acad. Sci. USA*, **99**, 16742–16747.
3. Lührs, T., Ritter, C., Adrian, M., Riek-Loher, D., Bohrmann, B., Döbeli, H. *et al.* (2005). 3D structure of Alzheimer's amyloid-beta(1–42) fibrils. *Proc. Natl Acad. Sci. USA*, **102**, 17342–17347.
4. Nelson, R., Sawaya, M., Balbirnie, M., Madsen, A., Riekel, C., Grothe, R. & Eisenberg, D. (2005). Structure of the cross-beta spine of amyloid-like fibrils. *Nature*, **435**, 773–778.
5. Ferguson, N., Becker, J., Tidow, H., Tremmel, S., Sharpe, T., Krause, G. *et al.* (2006). General structural motifs of amyloid protofilaments. *Proc. Natl Acad. Sci. USA*, **103**, 16248–16253.
6. Fändrich, M. (2007). On the structural definition of amyloid fibrils and other polypeptide aggregates. *Cell. Mol. Life Sci.* **64**, 2066–2078.
7. Bucciantini, M., Giannoni, E., Chiti, F., Baroni, F., Formigli, L., Zurdo, J. *et al.* (2002). Inherent toxicity of aggregates implies a common mechanism for protein misfolding diseases. *Nature*, **416**, 507–511.
8. Lashuel, H. & Lansbury, P. (2006). Are amyloid diseases caused by protein aggregates that mimic bacterial pore-forming toxins? *Q. Rev. Biophys.* **39**, 167–201.
9. Haass, C. & Selkoe, D. (2007). Soluble protein oligomers in neurodegeneration: lessons from the Alzheimer's amyloid beta-peptide. *Nat. Rev. Mol. Cell Biol.* **8**, 101–112.
10. Knight, J. & Miranker, A. (2004). Phospholipid catalysis of diabetic amyloid assembly. *J. Mol. Biol.* **341**, 1175–1187.
11. Gorbenko, G. P. & Kinnunen, P. K. (2006). The role of lipid–protein interactions in amyloid-type protein fibril formation. *Chem. Phys. Lipids*, **141**, 72–82.
12. Kremer, J. J., Sklansky, D. J. & Murphy, R. M. (2001). Profile of changes in lipid bilayer structure caused by beta-amyloid peptide. *Biochemistry*, **40**, 8563–8571.
13. Volles, M. J., Lee, S. J., Rochet, J. C., Shtilerman, M. D., Ding, T. T., Kessler, J. C. & Lansbury, P. T. (2001). Vesicle permeabilization by protofibrillar alpha-synuclein: implications for the pathogenesis and treatment of Parkinson's disease. *Biochemistry*, **40**, 7812–7819.

14. Ambroggio, E. E., Kim, D. H., Separovic, F., Barrow, C. J., Barnham, K. J., Bagatolli, L. A. & Fidelio, G. D. (2005). Surface behavior and lipid interaction of Alzheimer beta-amyloid peptide 1–42: a membrane-disrupting peptide. *Biophys. J.* **88**, 2706–2713.
15. Aisenbrey, C., Borowik, T., Byström, R., Bokvist, M., Lindström, F., Misiak, H. *et al.* (2008). How is protein aggregation in amyloidogenic diseases modulated by biological membranes? *Eur. Biophys. J.* **37**, 247–255.
16. Lopes, D., Meister, A., Gohlke, A., Hauser, A., Blume, A. & Winter, R. (2007). Mechanism of islet amyloid polypeptide fibrillation at lipid interfaces studied by infrared reflection absorption spectroscopy. *Biophys. J.* **93**, 3132–3141.
17. Chi, E., Ege, C., Winans, A., Majewski, J., Wu, G., Kjaer, K. & Lee, K. (2008). Lipid membrane templates the ordering and induces the fibrillogenesis of Alzheimer's disease amyloid-beta peptide. *Proteins*, **72**, 1–24.
18. Engel, M. F. M., Khemtmourian, L., Kleijer, C., Meeldijk, H., Jacobs, J., Verkleij, A. *et al.* (2008). Membrane damage by human islet amyloid polypeptide through fibril growth at the membrane. *Proc. Natl Acad. Sci. USA*, **105**, 6033–6038.
19. Caflisch, A. (2006). Computational models for the prediction of polypeptide aggregation propensity. *Curr. Opin. Chem. Biol.* **10**, 437–444.
20. Ma, B. & Nussinov, R. (2006). Simulations as analytical tools to understand protein aggregation and predict amyloid conformation. *Curr. Opin. Chem. Biol.* **10**, 445–452.
21. Gsponer, J., Haberthür, U. & Caflisch, A. (2003). The role of side-chain interactions in the early steps of aggregation: molecular dynamics simulations of an amyloid-forming peptide from the yeast prion Sup35. *Proc. Natl Acad. Sci. USA*, **100**, 5154–5159.
22. Klimov, D. K. & Thirumalai, D. (2003). Dissecting the assembly of Aβ_{16-22} amyloid peptides into antiparallel β sheets. *Structure*, **11**, 295–307.
23. Cecchini, M., Rao, F., Seeber, M. & Caflisch, A. (2004). Replica exchange molecular dynamics simulations of amyloid peptide aggregation. *J. Chem. Phys.* **121**, 10748–10756.
24. Hwang, W., Zhang, S., Kamm, R. & Karplus, M. (2004). Kinetic control of dimer structure formation in amyloid fibrillogenesis. *Proc. Natl Acad. Sci. USA*, **101**, 12916–12921.
25. Urbanc, B., Cruz, L., Yun, S., Buldyrev, S. V., Bitan, G., Teplow, D. B. & Stanley, H. E. (2004). In silico study of amyloid beta-protein folding and oligomerization. *Proc. Natl Acad. Sci. USA*, **101**, 17345–17350.
26. López de la Paz, M., de Mori, G. M., Serrano, L. & Colombo, G. (2005). Sequence dependence of amyloid fibril formation: insights from molecular dynamics simulations. *J. Mol. Biol.* **349**, 583–596.
27. Cecchini, M., Curcio, R., Pappalardo, M., Melki, R. & Caflisch, A. (2006). A molecular dynamics approach to the structural characterization of amyloid aggregation. *J. Mol. Biol.* **357**, 1306–1321.
28. Pellarin, R. & Caflisch, A. (2006). Interpreting the aggregation kinetics of amyloid peptides. *J. Mol. Biol.* **360**, 882–892.
29. Pellarin, R., Guarnera, E. & Caflisch, A. (2007). Pathways and intermediates of amyloid fibril formation. *J. Mol. Biol.* **374**, 917–924.
30. Linse, S., Cabaleiro-Lago, C., Xue, W., Lynch, I., Lindman, S., Thulin, E. *et al.* (2007). Nucleation of protein fibrillation by nanoparticles. *Proc. Natl Acad. Sci. USA*, **104**, 8691–8696.
31. Sharp, J., Forrest, J. & Jones, R. (2002). Surface denaturation and amyloid fibril formation of insulin at model lipid-water interfaces. *Biochemistry*, **41**, 15810–15819.
32. Jayasinghe, S. & Langen, R. (2007). Membrane interaction of islet amyloid polypeptide. *Biochim. Biophys. Acta*, **1768**, 2002–2009.
33. Murphy, R. (2007). Kinetics of amyloid formation and membrane interaction with amyloidogenic proteins. *Biochim. Biophys. Acta*, **1768**, 1923–1934.
34. Green, J., Kreplak, L., Goldsbury, C., Li Blatter, X., Stolz, M., Cooper, G. *et al.* (2004). Atomic force microscopy reveals defects within mica supported lipid bilayers induced by the amyloidogenic human amylin peptide. *J. Mol. Biol.* **342**, 877–887.
35. Kayed, R., Sokolov, Y., Edmonds, B., McIntire, T., Milton, S., Hall, J. & Glabe, C. (2004). Permeabilization of lipid bilayers is a common conformation-dependent activity of soluble amyloid oligomers in protein misfolding diseases. *J. Biol. Chem.* **279**, 46363–46366.
36. Cohen, F. & Kelly, J. (2003). Therapeutic approaches to protein-misfolding diseases. *Nature*, **426**, 905–909.
37. Shoval, H., Lichtenberg, D. & Gazit, E. (2007). The molecular mechanisms of the anti-amyloid effects of phenols. *Amyloid*, **14**, 73–87.
38. Jahn, T. R., Parker, M. J., Homans, S. W. & Radford, S. E. (2006). Amyloid formation under physiological conditions proceeds via a native-like folding intermediate. *Nat. Struct. Mol. Biol.* **13**, 195–201.
39. Cooke, I. & Deserno, M. (2005). Solvent-free model for self-assembling fluid bilayer membranes: stabilization of the fluid phase based on broad attractive tail potentials. *J. Chem. Phys.* **123**, 224710.
40. Ryckaert, J.-P., Ciccotti, G. & Berendsen, H. J. C. (1977). Numerical integration of the Cartesian equations of motion of a system with constraints: molecular dynamics of n-alkanes. *J. Comput. Phys.* **23**, 327–341.
41. Brooks, B. R., Bruccoleri, R. E., Olafson, B. D., States, D. J., Swaminathan, S. & Karplus, M. (1983). Charmm: a program for macromolecular energy, minimization, and dynamics calculations. *J. Comput. Chem.* **4**, 187–217.